Solution Structure of the Ribosome Recycling Factor from *Aquifex aeolicus*‡

Takuya Yoshida,§ Susumu Uchiyama,|| Hiroaki Nakano,§ Hiromasa Kashimori,§ Hiroyuki Kijima,§ Tamiko Ohshima,§ Yukari Saihara,§ Tetsuya Ishino,|| Hideto Shimahara,§ Toshio Yoshida,|| Kazuteru Yokose,|| Tadayasu Ohkubo,§ Akira Kaji,⊥ and Yuji Kobayashi*,§

Graduate School of Pharmaceutical Sciences, Osaka University, 1-6 Yamadaoka, Suita, Osaka 565-0871, Japan, RRF Research Inc., 1-25-14 Kannondai, Tsukuba, Ibaraki 305-0856, Japan, and Department of Microbiology, School of Medicine, University of Pennsylvania, Philadelphia, Pennsylvania 19104

Received October 25, 2000

ABSTRACT: The solution structure of ribosome recycling factor (RRF) from hyperthermophilic bacterium, *Aquifex aeolicus*, was determined by heteronuclear multidimensional NMR spectroscopy. Fifteen structures were calculated using restraints derived from NOE, J-coupling, and T_1/T_2 anisotropies. The resulting structure has an overall L-shaped conformation with two domains and is similar to that of a tRNA molecule. The domain I (corresponding to the anticodon stem of tRNA) is a rigid three α-helix bundle. Being slightly different from usual coiled-coil arrangements, each helix of domain I is not twisted but straight and parallel to the main axis. The domain II (corresponding to the portion with the CCA end of tRNA) is an α/β domain with an α-helix and two β-sheets, that has some flexible regions. The backbone atomic root-mean-square deviation (rmsd) values of both domains were 0.7 Å when calculated separately, which is smaller than that of the molecule as a whole (1.4 Å). Measurement of ^{15}N-{^{1}H} NOE values show that the residues in the corner of the L-shaped molecule are undergoing fast internal motion. These results indicate that the joint region between two domains contributes to the fluctuation in the orientation of two domains. Thus, it was shown that RRF remains the tRNA mimicry in solution where it functions.

Structures of ribosome and its subunits have been elucidated by cryo-electron microscopy and X-ray analysis on their crystals (*1*). The X-ray crystallography (*2*−*4*) showed the overall arrangement of the proteins and RNAs in the ribosome providing the location of the three essential sites, aminoacyl-tRNA binding (A-site), peptidyl-tRNA binding (P-site), and exit (E-site) sites. Furthermore, recent crystallographic studies revealed the crystal structure of both ribosomal subunits at very high resolutions (*5*−*7*).

On the other hand, soluble proteins involved in the translation process were elucidated at atomic resolution by X-ray crystallography and NMR spectroscopy (*8*−*11*). The X-ray analysis on the ternary complex of aminoacyl-tRNA, EF-Tu, and GTP analogue (*12*) in comparison with EF-G (*13*) presented a remarkable similarity between their structures.

At the termination step of protein biosynthesis, RF1 or RF2 (release factor 1 or 2) recognizes the stop codon on mRNA and then promotes the hydrolysis of peptidyl-tRNA at the P-site of the ribosome to release the nascent peptide chain. After the hydrolysis of peptidyl tRNA, followed by release of RF1 or RF2 from A site of ribosome by the action of RF3, the so-called posttermination complex, composed of 70S ribosome, deacylated tRNA, and mRNA, remains. The 70S ribosome is then dissociated into its subunits either after (*14*) or simultaneous with (*15*) the release from mRNA. In 1970, Kaji and co-workers found a protein that catalyzes the breakdown of the post termination complex into 70S ribosomes, tRNA and mRNA. They named it as the ribosome recycling factor (RRF)[1] (*16*, *17*). [First it was called ribosome releasing factor, but it was renamed as ribosome recycling factor to avoid confusion with peptide release factor, RFs (*18*).] A model posttermination complex, polysome treated with puromycin, was disassembled into 70S monosomes, mRNA and tRNA by RRF and EF-G. It has also been shown that, in the absence of RRF, ribosomes reinitiate to translate the 3′ portion of the mRNA downstream from the termination codon (*19*, *20*). Recently, in vitro studies on the mechanism of the RRF action was performed using a synthetic polynucleotide with poly-A tail and strong Shine Dalgarno (SD) sequence close by the termination codon (*21*−*23*). It was found in this system that 50S subunit is dissociated from the 70S ribosome complex during the disassembly process. The remaining complex of tRNA, mRNA, and 30S subunit is separated by IF3. In contrast, with natural mRNA (*24*, *25*), or with synthetic mRNA without the SD sequence (*26*), no ribosome remained on the mRNA. This indicates that the behavior of ribosomes in response to the action of RRF is very much dependent on the sequence of the mRNA surrounding the termination codon as demonstrated in vivo recently (*27*).

‡ Atomic coordinates have been deposited in the Protein Data Bank (accession code 1GE9).

* To whom correspondence should be addressed. Phone: +81-6-6879-8220. Fax: +81-6-6879-8224. E-mail: yujik@protein.osaka-u.ac.jp.

§ Osaka University.

|| RRF Research Inc.

⊥ University of Pennsylvania.

[1] Abbreviations: RRF, ribosome recycling factor; NMR, nuclear magnetic resonance; HSQC, heteronuclear single quantum coherence spectroscopy; NOE, nuclear overhauser effect; EF-G, elongation factor G; tRNA, transfer RNA; GTP, guanine nucleotide triphosphate; rmsd, root-mean-square deviation; T_1, spin−lattice relaxation time; T_2, spin−spin relaxation time.

10.1021/bi002474g CCC: $20.00
Published on Web 02/20/2001

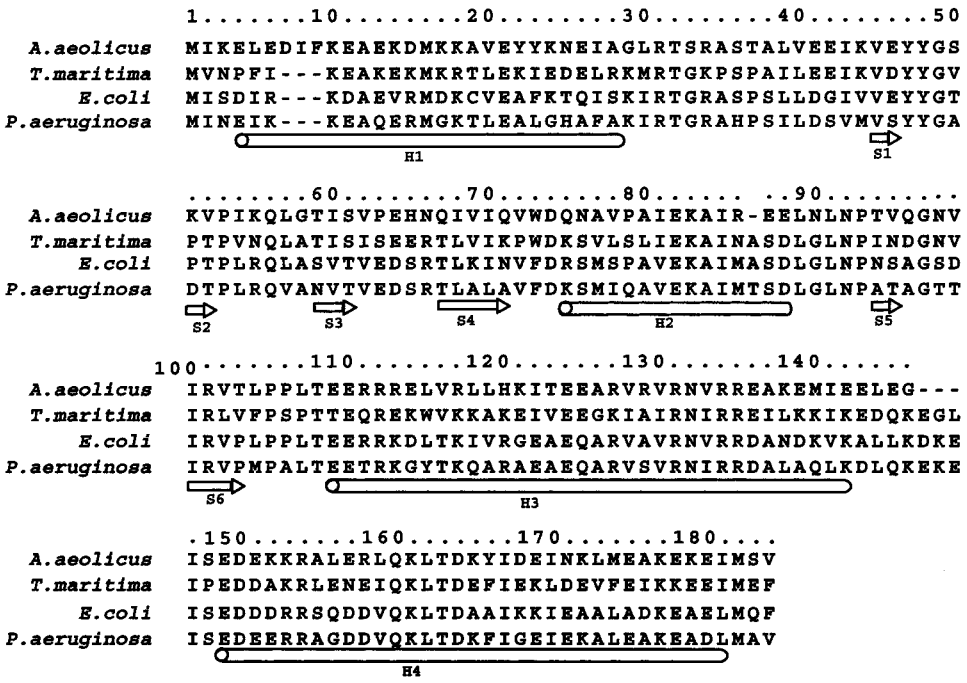

FIGURE 1: Multiple sequence alignment of RRFs. The numbering and location of secondary structure elements correspond to the *A. aeolicus* structure.

In our attempt to elucidate the structure of RRF with the NMR techniques, the secondary structure of RRF from *Pseudomonas aeruginosa* was elucidated, and it was shown that the molecule is characterized by three long α-helices (*28*). In this paper, we report the three-dimensional structure of RRF from *Aquifex aeolicus* in solution as determined by NMR. We confirmed the crystal structure of *Thermotorga maritima* RRF, L-shaped conformation with the domains, which has been suggested to mimic tRNA (*29*). The solution structure of *A. aeolicus* RRF is similar also to the crystal structure of *Escherichia coli* RRF except for the angle of two domains (*30*).

EXPERIMENTAL PROCEDURES

Expression and Purification. The DNA fragment encoding RRF sequence (Figure 1) was amplified by PCR using *Aquifex aeolicus* genome DNA (*31*) as a template. This was kindly supplied as a gift by R. Huber (Universität Regensburg, Germany). The PCR product was cloned into the pET22b(+) plasmid vector (Novagen, Madison, WI). The construct, pETARRF, was introduced into *E. coli* strain BL21(DE3). Uniformly ^{15}N and ^{13}C-labeled protein was obtained by growing the cells in M9 medium containing [^{13}C]-glucose (2 g/L) and/or [^{15}N]ammonium chloride (1 g/L) as the sole carbon and nitrogen sources. Uniform ^{2}H labeling was obtained using M9 medium containing 99% D_2O. The cells were grown at 37 °C in M9 medium to $A_{600} = 0.5$ and the protein expression was induced by adding isopropyl-1-thio-β-D-galactopyranoside (IPTG) to a final concentration of 1.0 mM, followed by 4 h incubation. Harvested cells were suspended in buffer A [50 mM Tris-HCl, pH 8.0, 50 mM NaCl, 1 mM EDTA, 1 mM (4-amidinophenyl)-methanesulfonyl fluoridehydrochloride monohydrate (APMSF)] and disrupted by sonication. The homogenate was centrifuged to remove the insoluble debris. The supernatant was heated at 80 °C for 10 min and centrifuged. The heat treatment step simplified the purification procedure and decreased the protein loss because the majority of contaminating cellular proteins were denatured and precipitated. The supernatant was dialyzed against buffer B (50 mM Tris-HCl, pH 8.0, 50 mM NaCl), the solution was applied to a DEAE-sepharose (Amersham Pharmacia Biotech, Uppsala, Sweden) column equilibrated with buffer B, and flow through fractions were collected. Fractions containing *A. aeolicus* RRF were confirmed by SDS−PAGE and concentrated using ultrafiltration (YM-10, Millipore, Bedford, MA), followed by purification by Superdex 75pg column (Amersham Pharmacia Biotech, Uppsala, Sweden) equilibrated with buffer B. *A. aeolicus* RRF was purified to homogeneity as judged by SDS−PAGE. The NMR samples of [*U*-^{15}N]RRF, [*U*-^{15}N/^{13}C]RRF, [*U*-^{2}H/^{15}N/^{13}C]RRF, and [*U*-10% ^{13}C]RRF were prepared in 93% H_2O/7% D_2O or 99.9% D_2O sodium acetate buffer of 20 mM at pH 5.2 with 20 mM NaCl. The protein concentration was determined spectrometrically using the molar extinction coefficient of 14 300 cm^2 mol^{-1}, and the solutions of 0.4−0.5 mM were used for NMR measurements.

NMR Spectroscopy. NMR experiments were carried out at 40 °C on Varian INOVA600 or INOVA500 spectrometers equipped with shielded gradient triple resonance probes. Pulsed-field gradient technique with a WATERGATE (*32*) or a Rance-Kay method (*33*) was used for all H_2O experiments. Transmitter frequencies for ^{1}H, ^{15}N, ^{13}Cα, aliphatic ^{13}C, aromatic ^{13}C, and carbonyl ^{13}C were typically 4.76, 119.0, 55.0, 43.0, 125.0, and 176 ppm, respectively. Proton chemical shifts were referenced with sodium 4,4-dimethyl-4-silapentane-1-sulfonate (DSS). ^{15}N and ^{13}C chemical shifts were indirectly referenced according to gyromagnetic ratio (*34*). ^{15}N-^{1}H-HSQC, ^{15}N-separated NOESY-HSQC, and ^{15}N-separated TOCSY spectra were acquired on [*U*-^{15}N]RRF. HNCO, HNCA, CBCANH, CBCA(CO)NH, HBHA(CBCA-CO)NH, H(CCO)NH, HCCH-TOCSY, HCCH-COSY, ^{13}C-^{1}H HSQC, (Hβ)Cβ(CγCδ)Hδ, ^{13}C-separated NOESY-HSQC, J-modulated HSQC spectra were acquired on [*U*-^{15}N/^{13}C]RRF. HN(CA)CO, C(CO)NH, and ^{15}N-separated HMQC-

NOESY-HSQC spectra were acquired on [*U*-^{2}H/^{15}N/^{13}C]RRF. Other experimental details, together with the original references, are provided in the reviews (*35, 36*). The mixing times employed for NOE experiments were 75 ms except for 3D ^{15}N-separated HMQC-NOESY-HSQC, for which 150 ms was used. A constant time HSQC was acquired on [*U*-10% ^{13}C]-RRF. Slowly exchanging ^{1}HN were identified from a series of ^{15}N-HSQC spectra following a rapid buffer exchange to 99% D_2O using a NAP-5 column (Amersham Pharmacia Biotech, Uppsala). Processing of the data was carried out using the NmrPipe software package (*37*). For analysis of the multidimensional spectra, PIPP/CAPP/STAPP (*38*) and in-house written programs were used.

The backbone ^{15}N relaxation parameters comprising the ^{15}N longitudinal relaxation time T_1, transverse relaxation time T_2 and ^{15}N-{^{1}H} NOE, were measured using HSQC type pulse sequences. The T_1 relaxation decay was sampled at six time points (30, 234, 438, 642, 846, and 1050 ms) and the $T_1\rho$ decay was sampled at five points (12, 24, 36, 48, and 60 ms) using a ^{15}N spin-lock field strength of 2.2 kHz. The ^{15}N-{^{1}H} NOE values were derived from two series of spectra, recorded with and without 3.5 s of saturation of the amide protons, respectively. All data were recorded in an interleaved manner in order to minimize the effects of spectrometer drift. The ^{15}N-{^{1}H} NOE values were corrected for the finite delay between scans using T_1 values of ^{1}HN, which were estimated by a preliminary experiment (*39*). The T_1 and $T_1\rho$ values were obtained by nonlinear least-squares fitting of a two-parameter monoexponential function through the peak intensities, using the Levenberg−Marquardt algorithm (*40*). The T_2 values were calculated from T_1 and $T_1\rho$ with the resonance offset frequencies and the strength of the spin-lock field (*41*). Uncertainties in T_1 and $T_1\rho$ values were estimated from the covariance matrix of a least-squares fit. And those in NOE values were estimated by simple error propagation calculation based on baseplane rms noise in spectra.

Structure Calculations. NOEs were classified as strong, medium, weak, or very weak, corresponding to distance restraints of 1.8−2.7 Å (1.8−2.9 Å for NOEs involving amide protons), 1.8−3.3 Å (1.8−3.5 Å for NOEs involving amide protons), 1.8−5.0 and 1.8−6.0 Å, respectively (*42*). For distances involving methyl groups, methylene protons and aromatic ring protons, $\langle r^{-6}\rangle^{-1/6}$ averaged distances were used (*43*). Protein backbone hydrogen-bonding restraints (two per hydrogen bond: one between the amide proton and the carbonyl oxygen of 1.5−2.8 Å and one between the amide nitrogen and the carbonyl oxygen of 2.4−3.5 Å) were introduced (*44*). To collect all the distance restraints, an iterative refinement strategy (*45*) was employed. The program TALOS (*46*) was used to derive the backbone φ and ψ torsion angle restraints based on chemical shifts of Cα, Cβ, C′, Hα, and N. The TALOS-derived torsion angles are empirical and may contain a few errors. Therefore, the sufficiently larger ranges (±30°) were employed for TALOS-derived restraints in the initial round of calculation. In the final round of calculation, after the structures were well defined and erroneous restraints were excluded, the minimum ranges employed for φ and ψ were reduced to ±1.5 × SD, where SD is the standard deviation for predicted values. χ_1 angles for aromatic residues and for Ile, Thr, and Val residues were derived from $^{3}J_{C\gamma N}$ and $^{3}J_{C\gamma CO}$ coupling constants (*47, 48*). The minimum ranges employed for χ_1 were ±20°.

The preliminary structure calculation using restraints of NOE-derived interproton distances and torsion angles indicated that the structure of *A. aeolicus* RRF has a highly anisotropic prolate shape. Since the anisotropy of the molecule was also shown in the observed profile of T_1 and T_2 data, we employed the dependence of T_1/T_2 on the rotational diffusion anisotropy as restraints for further structure refinement procedure. The diffusion anisotropy restraints were derived as follows: The initial diffusion tensor was estimated from the examination of histogram of ^{15}N T_1/T_2 ratios for isotropically oriented vectors (*49*). After calculating an ensemble of structures, the diffusion tensor and its unique axis were refined by simplex nonlinear optimization to fit the observed T_1/T_2 ratios to the calculated T_1/T_2 ratios derived from structures. In this procedure, a fully asymmetric diffusion tensor was used. The structures were calculated using the program CNS (*50*) with torsion angle dynamics (*51*) followed by a simulated annealing refinement on a Linux workstation with Cerelon 400 MHz. The final structures were analyzed using the programs of MOLMOL (*52*) and PROCHECK (*53*).

RESULTS

Resonance Assignments. Sequential assignments for backbone ^{15}N, ^{1}H^{N},^{13}Cα, and side chain ^{13}Cβ nuclei were obtained from analysis of ^{15}N-^{1}H-HSQC, HNCA, CBCANH, and CBCA(CO)NH spectra. These assignments were confirmed in the analysis of HNCO and HN(CA)CO spectra. Figure 2 shows the ^{15}N-^{1}H-HSQC spectrum of RRF with assignments for the cross-peaks indicated as residue number. Complete assignments of the backbone ^{1}H^{N}, ^{15}N, ^{13}Cα, and ^{13}C′, except for ^{1}H^{N} and ^{15}N of Leu5, were achieved. The amide resonance of Leu5 was not observed presumably due to the conformational exchange of the molecule. Backbone assignments were extended to the side chain. Hα/β resonances were assigned in HBHA(CBCACO)NH and ^{15}N-separated TOCSY-HSQC spectra. Other aliphatic ^{13}C and ^{1}H side-chain assignments were obtained mainly from C(CO)NH and H(CCO)NH spectra. Because of the relatively low sensitivities for these experiments, HCCH-TOCSY and HCCH-COSY spectra were employed to complement them. Aromatic side-chain assignments were obtained from (Hβ)Cβ(CγCδ)Hδ spectrum. Most ^{1}H and ^{13}C resonances of the side chain were assigned. In some cases, side-chain resonances of residues with longer side chains could not be assigned unambiguously because of overlapping signals. Stereospecific assignments for prochiral methyl resonances of Leu and Val were obtained in constant-time HSQC spectrum recorded on [*U*-10% ^{13}C]RRF (*54*). No stereospecific assignment for methylene protons was obtained.

T_1/T_2 Restraints. T_1, T_2, and ^{15}N-{^{1}H} NOE values for 139 out of 173 assigned backbone nitrogen nuclei were analyzed to derive T_1/T_2 restraints, whereas peak overlap prevented the analysis of cross-peaks for 34 residues. In the absence of significant internal motions, the ^{15}N T_1/T_2 ratio provides the long-range structural information in the form of internal ^{15}N-^{1}H vector constraints with respect to an overall molecular reference frame. Residues with large-amplitude internal motions on subnanosecond time scale were recognized by significant decreases in ^{15}N-{^{1}H} NOE values. Thirty one

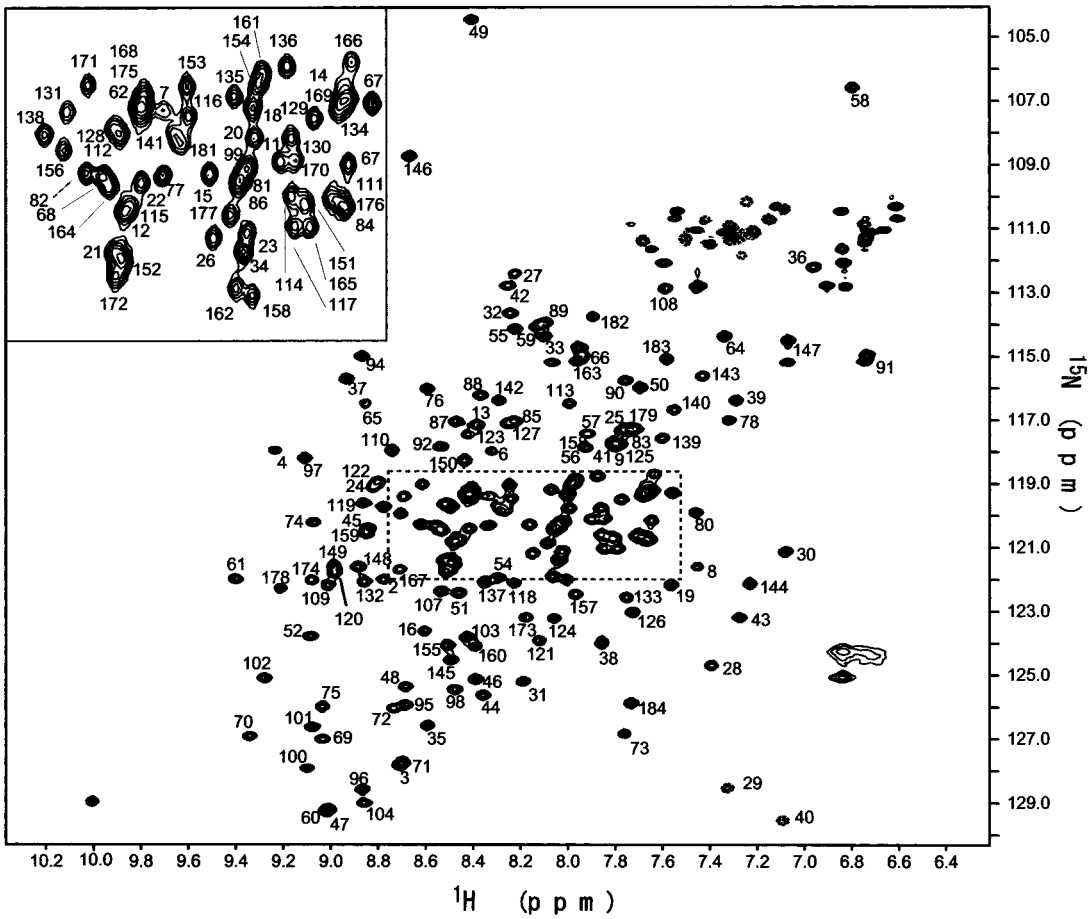

FIGURE 2: ^{1}H-^{15}N HSQC spectrum of *A. aeolicus* RRF with assignments for the cross-peaks indicated as residue numbers. Complete assignments of the backbone amide groups, except for Leu5, were achieved. The cross-peaks for Gly29 and Val40 are aliased along the ^{15}N dimension.

residues which showed low ^{15}N-{^{1}H} NOE values (<0.65) were excluded in the analysis of diffusion tensor (*56*). Furthermore, residues undergoing conformational exchange, which can be characterized by $[(\langle T_2\rangle - T_2)/\langle T_2\rangle] - [(\langle T_1\rangle - T_1)/\langle T_1\rangle] > 1.5 \times$ SD, can be excluded, where SD is the standard deviation of the left-hand side of the equation and $\langle T_1\rangle$ and $\langle T_2\rangle$ are the average values of T_1 and T_2, respectively (*55*). However, such residues were not found in *A. aeolicus* RRF. T_1 and T_2 values of 108 NH cross-peaks were utilized to derive an anisotropic rotational diffusion tensor and T_1/T_2 restraints (Figure 3a). The histogram of T_1/T_2 (Figure 3b) had a bimodal profile and the maximum of the T_1/T_2 ratio was about 3.2 times larger than the minimum ratio. Initial estimates of the effective correlation time, anisotropy and rhombicity from the analysis of a histogram of T_1/T_2 ratios using a fully anisotropic diffusion model, were 13.4 ns, 2.75 and 0.25, respectively. The value of anisotropy is found to be sufficiently large to employ the T_1/T_2 restraints. Thus, this method has been justified for structure elucidation of *A. aeolicus* RRF.

Structure Determination. A total of 1687 distance restraints derived from NOE experiments were employed for structure calculations, including 549 intraresidue, 496 sequential, 386 medium-range, and 256 long-range restraints. In addition, 98 H^N-O and N−O hydrogen bond restraints were used in the later stages of the structure calculation. Torsion angle restraints comprised 25 χ_1 restraints derived from semiquantitative analysis of $^{3}J_{C\gamma N}$ and $^{3}J_{C\gamma CO}$ and 301 φ/ψ angle restraints calculated by the program TALOS. Figure 4a shows the best-fit superpositions of the backbone traces of 15 structures of *A. aeolicus* RRF obtained by the simulated annealing refinement. The ensemble of 15 structures has no distance restraint violations above 0.5 Å, and no torsion angle restraint violations above 5°. The structure statistics are summarized in Table 1. The Ramachandran plot shows that 86.0% of the nonglycine and nonproline residues are found in the most favored region, 11.7% in the additionally allowed regions.

The lowest energy structure among the 15 final structures is shown as a ribbon representation in Figure 5a. The resulting structure of *A. aeolicus* RRF has an L-shaped conformation with two domains. The overall structure is very similar to that of tRNA (Figure 5b) in shape with nearly the same dimension. Domain I, the leg portion of the molecule corresponding to the vertical line of L, is a three-stranded antiparallel α-helix bundle with length of 60 Å consisting of residues 4−28 (helix 1), 109−142 (helix 3), and 149−181 (helix 4). Each helix is nearly straight and packed together in a slightly right-handed twist with helix-crossing angle of 5°. The H−N vectors of peptide plane in the three-helix bundle are nearly parallel to the principal axis of anisotropic diffusion tensor of RRF molecule. The helices in domain I have amphiphilic properties and the constituting hydrophobic residues are positioned at the inner-face as usually seen in a helix bundle. Domain II, the foot portion of molecule corresponding to the horizontal line of L, of

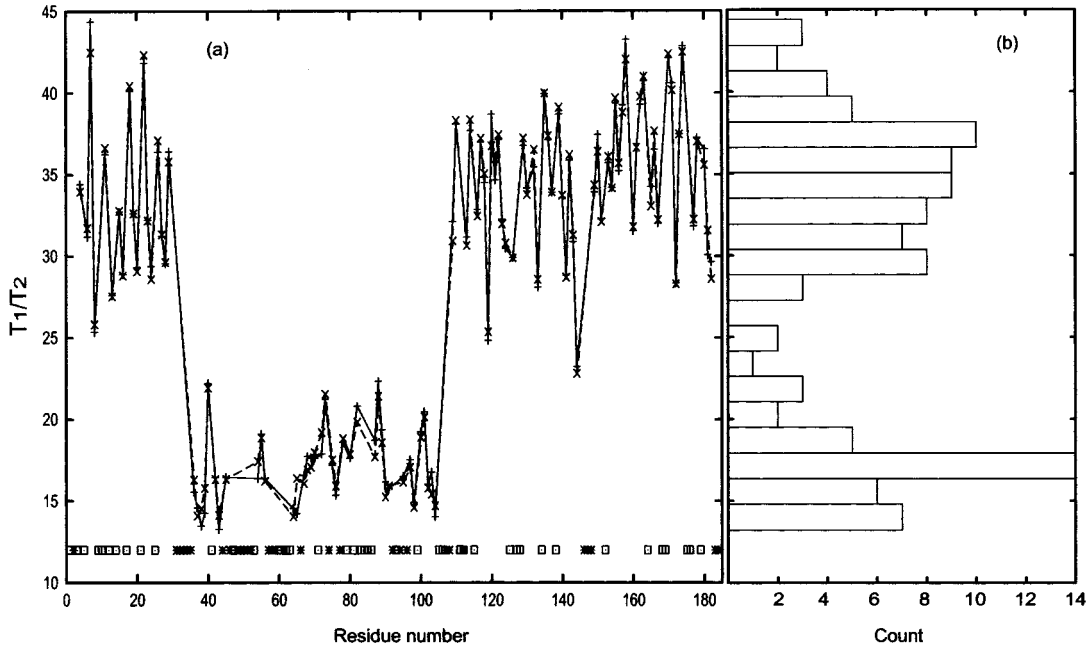

FIGURE 3: (a) Observed (+) and calculated (×) T_1/T_2 ratios versus residue number. Residues with low ^{15}N-{^{1}H} NOE values (<0.65), which were excluded in the analysis of rotational diffusion anisotropy, are indicated by asterisks. Residues with resonance overlap and proline residues are indicated by open-boxes. (b) The histogram of observed T_1/T_2 ratios. The range of T_1/T_2 ratios are divided into twenty bins. The counts of T_1/T_2 ratio in each bin are shown.

which instep is 30 Å long, is a three-layer $\beta/\alpha/\beta$ sandwich consisting of an α-helix (helix 2, residues 75−88), a two-stranded short antiparallel β-sheet (strand 1 and strand 2, residues 45−46 and 51−52) and a four-stranded antiparallel β-sheet (strand 3 and strand 4, residues 59−61 and 67−71; strand 5 and strand 6, residues 94−95 and 100−103). Strand 5 and strand 6 are connected by a β-turn. The toe of domain II is composed of the β-turn and two turns linking strand 1 and strand 2, and helix 2 and strand 4. The four-stranded antiparallel β-sheet has an amphiphilic profile and forms the hydrophobic core with helix 2. In the tripeptide 37−39 region of domain II, backbone torsion angles show that these three residues are fit in a helical conformation, which coincide with the indication in the chemical shift data. This helical region was also indicated from the NMR analysis of *P. aeruginosa* RRF (*28*) and observed in the X-ray structure of *T. maritima* RRF (*29*).

Orientation of Two Domains. As shown in Figure 4, panels b and c, the ensembles of structures were converged well individually. The average atomic root-mean-square deviation (rmsd) values for backbone atoms of both domains were 0.7 Å. On the other hand, the rmsd value for the whole molecule was substantially larger (1.4 Å). The relative orientation between two rigid bodies is given by the set of three spherical polar angles: Φ, ϑ,and X as shown in Figure 6. In this study, the *z*-axis of reference frame of domain I is defined by the long axis of three-helix bundle, and its *x*-axis is set along the vector connecting the center of three-helix bundle to helix 1. On the other hand, the *z*′-axis of domain II is defined by the long axis of strand 5 and the *x*′-axis is set along the vector between strand 5 and helix 2. The average values of Φ, ϑ, and X, are 4.3°, 89.7°, and −62.6°, respectively. The standard deviations of zenith angles, ϑ, and rotation angles of *x*′-axis around *z*′-axis, X, fall in narrow ranges (±4.5° and ±7.4°). But the standard deviation of azimuth angles, Φ, spans rather a wide range of ±17.4°.

DISCUSSION

Recently, crystal structures of RRF from two different bacteria have been elucidated (*29*, *30*). They are from hyperthermophilic bacterium, *Thermotoga maritima*, and from mesophilic bacterium, *E. coli*. Both structures are almost similar to each other except for the angle between two domains and characterized by their overall profiles of an L-shaped conformation. The contact of the two domains is accompanied by an 8.2% (981 Å^2) loss in water-accessible surface area (*ASA*) in *T. maritima* RRF (*29*). As judged from the published results of *E. coli* RRF (*30*), loss in *ASA* due to domain contact is about the same or possibly even smaller than that of *T. maritima* RRF. These values are significantly smaller than those of usual domain interactions in which each domain forms stable binding to each other (*56*), suggesting weak interaction between the two domains of RRF molecule. Therefore, it is possible that packing forces or insertion of detergent molecule in the crystal is responsible for the difference between two structures of RRF.

The present result provides the structure of RRF in free state because *A. aeolicus* RRF was analyzed in solution free of crystal lattice restrains. Structure determination procedure by NMR usually relies on short range distance restraints. However, these restraints are not sufficient for the determination of the relative orientation of domains. We have tried a couple of new methods, which have been recently developed for defining the long-range order in NMR structure determination (*57*, *58*). These approaches utilize the information from the relaxation time dependence on rotational diffusion anisotropy or the residual dipolar coupling of weakly aligned molecules. In the present study, a well-converged structure could be elucidated through the relaxation time dependence approach. Figure 3 shows the agreement between the calculated and the observed ^{15}N T_1/T_2 ratios, which indicates that the T_1/T_2 anisotropy restraints

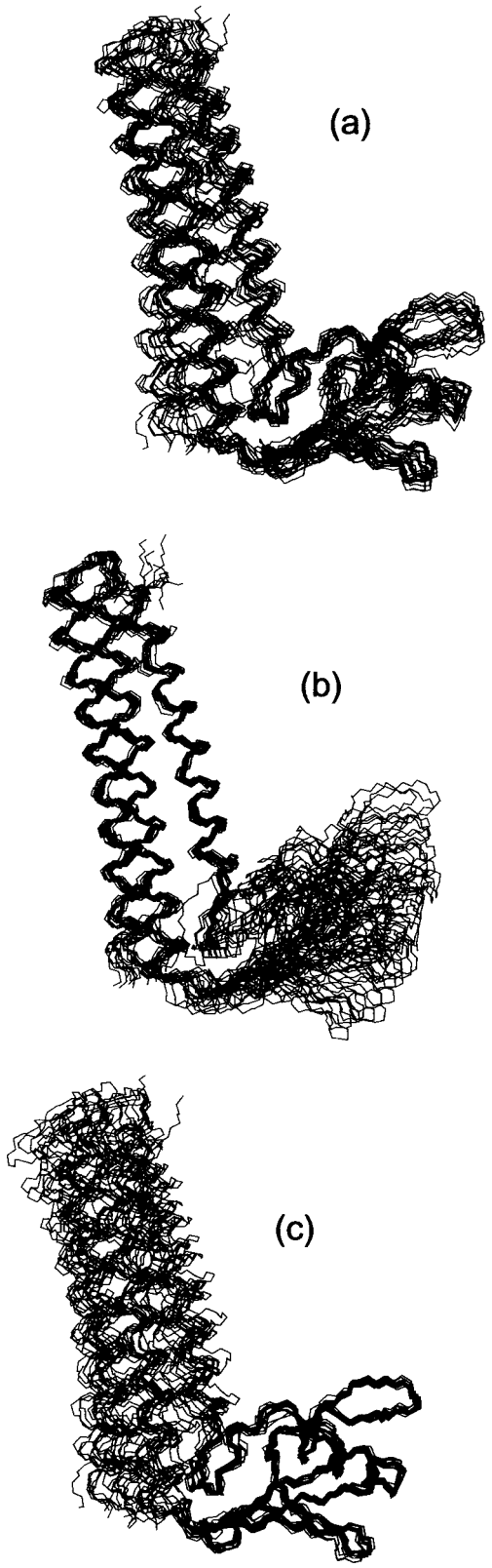

FIGURE 4: Best-fit superpositions of the backbone atoms of (a) whole molecule, (b) the domain I, and (c) the domain II of the 15 NMR-derived structures of *A. aeolicus* RRF. The rmsd values for backbone atoms of both domains were 0.7 Å, indicating that the ensembles of structures converged well individually. On the other hand, the rmsd values for the whole molecule were substantially larger than 1.4 Å.

are consistent with other restraints and reliable. Thus, we could conclude that the characteristic tRNA like conformation of RRF molecule is maintained in solution. This supports the notion that RRF mimics the function of tRNA (*29*).

Table 1: Structural Statistics for the Final Structures of *A. aeolicus* RRF[a]

	rmsd from experimental restrains
distances (Å)	0.015 ± 0.003
torsion angles (deg)	0.81 ± 0.06
T_1/T_2 ratios	0.88 ± 0.09
	rmsd from idealized covalent geometry
bonds (Å)	0.0198 ± 0.0002
angles (deg)	0.42 ± 0.03
impropers (deg)	0.45 ± 0.04
	coordinate precision
domain I (residues 5−29, 109−142, 149−180)	0.68
domain II (residues 30−108)	0.73
whole molecule (residues 5−142, 149−181)	1.42

[a] The final force constants employed for the various terms in the target function used for structure calculation are as follows: 1000 kcal mol^{-1} Å^{-2} for bond lengths, 500 kcal mol^{-1} rad^{-2} for angles and improper torsions (which serve to maintain planarity and chirality), 4 kcal mol^{-1} Å^{-4} for the quartic van der Waals repulsion term, 30 kcal mol^{-1} Å^{-2} for the experimental distance restraints, 200 kcal mol^{-1} rad^{-2} for the torsion angle restraints, and 1.0 kcal mol^{-1} for for the T_1/T_2 restraints. The precision of the atomic coordinates is defined as the backbone (C′, Cα, N) rmsd between the 15 final structures and the mean coordinates. The disorderd residues 1−4, 143−148, and 181−184 are excluded for the calculation.

The structures for each domain of *A. aeolicus* RRF are basically in agreement with those of *T. maritima* RRF and *E. coli* RRF (*29*, *30*). The backbone traces of domain I and domain II of *A. aeolicus* RRF can be superimposed on those of *T. maritima* RRF with rmsd values of 1.7 and 1.8 Å, respectively. The *ASA* loss of *A. aeolicus* RRF accompanied by the domain−domain interaction is 829 Å^2 (6.5%), which is close to the value of *T. maritima* RRF (*29*). The small value in the *ASA* loss indicates that the two domains contact each other through a small area that seems to be insufficient to fix the structural arrangement between them. The intrinsic structure of the joint region, which is composed of double polypeptide chains (Leu30−Ser36 and Leu104−Thr108) with proline residues (Pro105, 106) (Figure 1) that restrict the conformation of a polypeptide chain, may contribute to stabilize the tRNA like conformation of RRF in solution.

Regarding the relative orientations of two domains, differences among the three RRFs are found. The bending angle of the joint between the two domains (ϑ) in *A. aeolicus* RRF is 90° and seems to be significantly different from that of *E. coli* RRF (110°), but identical to *T. maritima* RRF (90°). As a result, *E. coli* RRF is an open L-shaped molecule rather than a strict L-shaped molecule. According to Kim et al. (*30*), this makes *E. coli* RRF not a near perfect mimic of tRNA in contrast to *T. maritima* RRF. The differences between *A. aeolicus* RRF and *T. maritima* RRF are found in the rotational direction of domain II around the long axis of domain I (Φ). The angle Φ varied 33 ± 17° (error range is defined by the standard deviation) when domain I of each RRF was superimposed (Figure 6). These comparisons suggest that the rotational angle of domain II (Φ) can vary

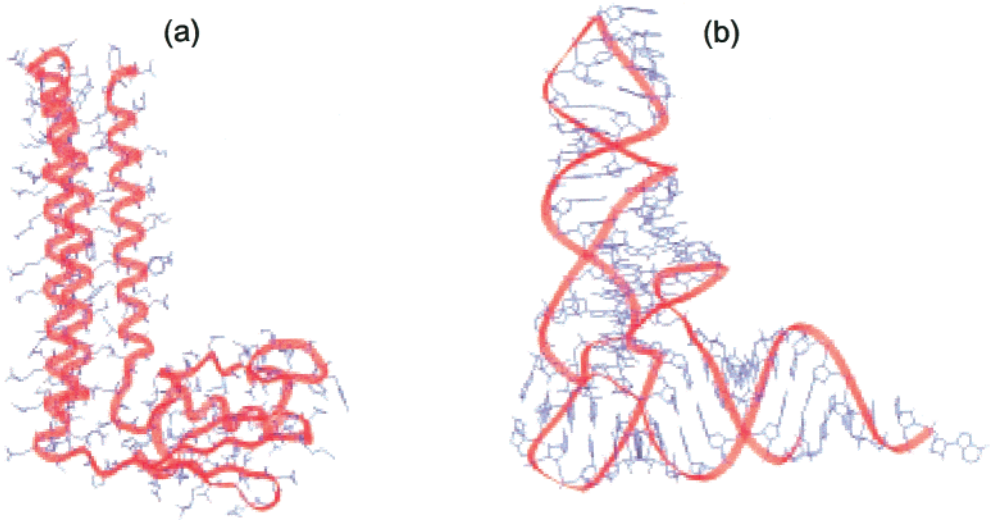

FIGURE 5: Schematic presentation of the structure of (a) *A. aeolicus* RRF and (b) $tRNA^{Phe}$.

in solution while the angle between the domains (ϑ) may vary under the stress of crystal lattice formation. It is important to point out that the relative rotation of two domains appears to occur maintaining ϑ equal to 90° or without much of rotation of X. It is possible that the relative movement of these two domains is functionally important as discussed in a recent paper (*59*). As shown in Figure 6, fluctuations of the relative orientation between domain I and II are observed in the ensemble of NMR structures. Such disorder originates from a lack of structural restraints that may be due to internal mobility of the joint region. The values of ^{15}N-{^{1}H} NOE clearly show the flexibility of the joint region of *A. aeolicus* RRF (Figure 8). Recently, the activities of RRFs from several bacteria were investigated in *E. coli*. *P. aerginosa* RRF was shown to be active in *E. coli* (*60*) while *T. maritima* RRF is toxic to *E. coli* (*59*). Furthermore, *T. thermophils* RRF failed to complement the lethal mutation of *E. coli* on the RRF gene while truncated RRF could (*61*). The C-terminal truncation of *E. coli* RRF has also been shown to cause temperature sensitivity of the molecule (*20*). These studies suggest that RRFs from thermophiles are able to bind to ribosome of *E. coli* but are inactive or less active in ribosome recycling assay performed at the room temperature. This is because RRFs from thermophiles were not endowed with the interdomain flexibility at the ambient temperature. Thus we could conclude that the domain movement is important for its action against the ribosome.

Structures of Domain I and Domain II. The three-helix bundle structure found in *A. aeolicus* RRF is different from those of classical left-handed coiled-coils. The helices of *A. aeolicus* RRF are nearly straight and packed together with an unusual right-handed twist. In classical coiled-coils, the heptad repeats, $(abcdefg)_n$, which is a 7-fold repeat in the primary sequences, contribute to stabilize the left-handed supercoil through hydrophobic interactions at position "a" and "d" (*62*). As shown in Figure 7a, in the case of RRF domain I, the autocorrelation of hydrophobicity in the primary sequence reveals undecad (11-fold) repeats of hydrophobic residues in addition to normal heptad. It is known that undecad repeats form a slightly right-handed supercoiled structure (*62*). Such mixture of heptad and undecad repeats may contribute to stabilize the characteristic straight three-helix bundle structure in RRF through hydrophobic interactions. The critical role of hydrophobic interactions at three-helix bundle on the stability is indicated in the study of temperature sensitive phenotype of *E. coli* RRF (*20*), in which a single mutation (shown in Figure 7b) of a hydrophobic residue in domain I influences the thermal stability of RRF.

Additionally, amino acid residues on the surface also modulate the stability of helices. Although no specific salt bridge (within 4.0 Å) was found in *A. aeolicus* RRF, the biased distribution of charged residues suggests that long-range electrostatic interactions may contribute to stability of RRF molecule. It has been reported that, compared to mesophiles, proteins of thermophiles show higher contents of charged amino acids (*63*), and that charged amino acids on surface of protein enhance thermostability (*64*). In case of thermophilic RRFs, the amount of charged residues (Asp, Glu, Arg, Lys, and His) within the residues of three-helix bundle are larger (e.g., 52%; *A. aeolicus*, 52%; *T. maritima*) than that of mesophiles (e.g., 47%; *E. coli*, 44%; *P. aeruginosa*).

Domain I has a well conserved surface which is mainly composed of residues in helix 3. This region has a cluster of positive charges, which is effective for interacting with the negative charge of the phosphate backbone of RNA. Any mutation of Arg110, Arg129, and Arg132 of *E. coli* RRF (corresponding to Arg112, Arg131, and Arg134 of *A. aeolicus* RRF, respectively) is lethal (*65*). This experimental result supports the hypothesis that the surface of helix 3 might be necessary to interact with rRNA.

In contrast to the rigid structure of domain I, domain II has several flexible regions, which are reflected by low ^{15}N-{^{1}H} NOE values (Figure 8). These results are consistent with the notion that domain II is the basic structure critical for maintaining the function of RRF. It is therefore understandable that several lethal mutations (for example, Leu65Pro) but no temperature sensitive mutations were found in this domain (*65*). It is known that the flexible region of a protein is essential for its function (*66*, *67*). It was noted that a conserved surface is located in the toe of domain II. This region consists of Tyr48, Trp73, and Asp74. These residues are unusually exposed to solvent and, therefore, may play a

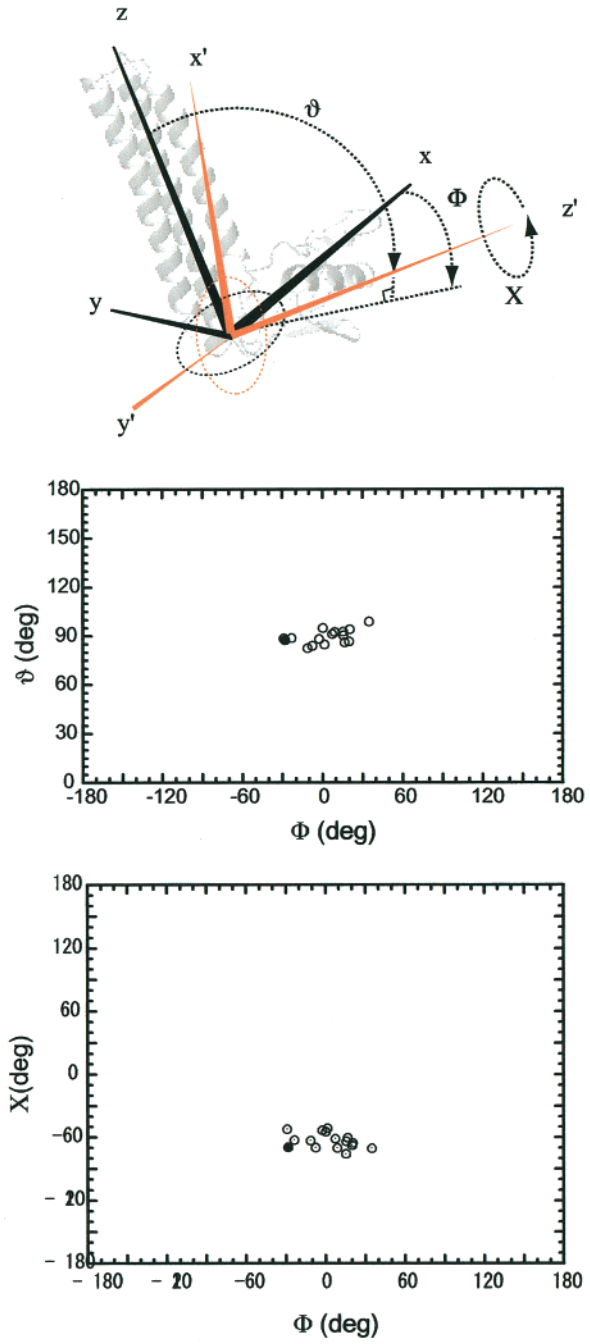

FIGURE 6: Distributions of interdomain angles for the ensemble of the 15 NMR-derived structures of *A. aeolicus* RRF (open circles), and for the X-ray structure of *T. maritima* RRF (closed circle). The interdomain angles are represented by the set of three spherical polar angles. The definitions for the angles are shown schematically (for detailed definitions, see the section of *orientation of two domains* in results). The average values of Φ, ϑ, and X, are 4.3°, 89.7°, and −62.6°, respectively. The standard deviations of Φ, ϑ, and X, are 17.4°, 4.5°, and 7.4°, respectively.

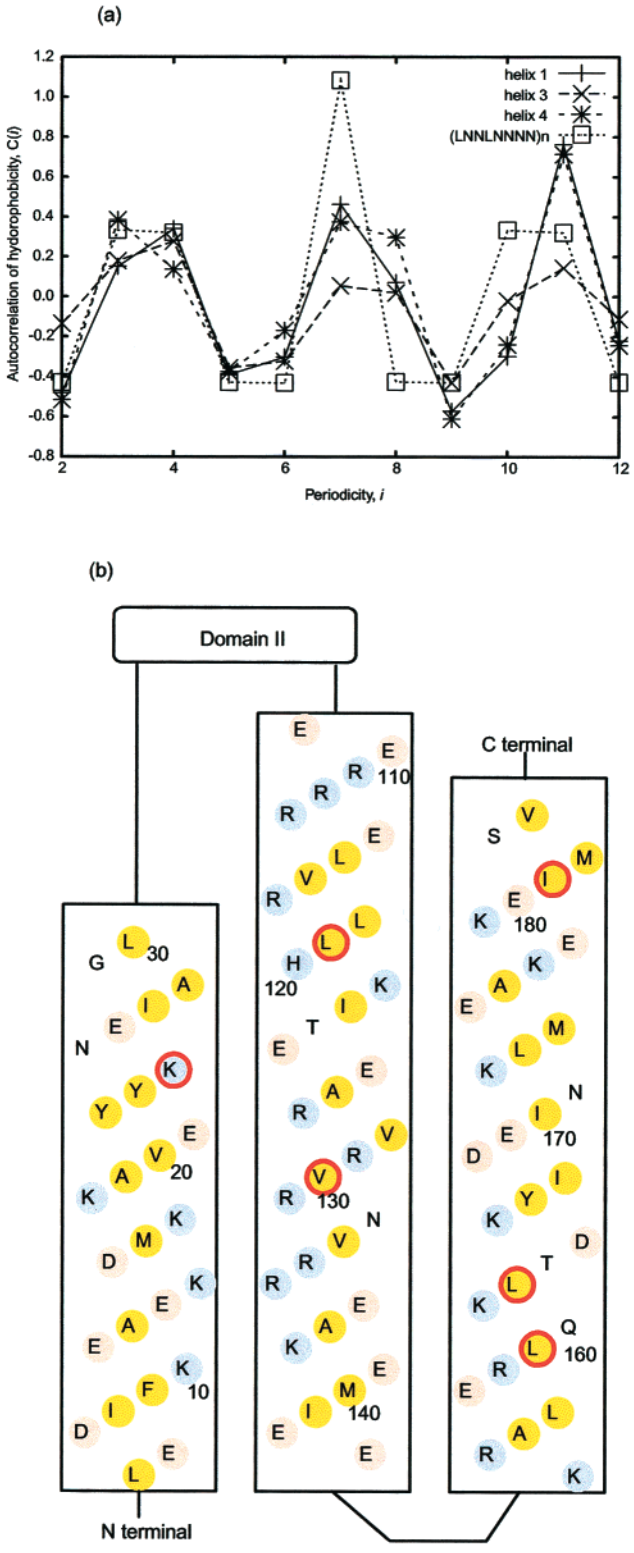

FIGURE 7: (a) Discrete autocorrelations, C(i), of hydrophobicity in the primary sequences [(+) helix 1, (×) helix 2, and (*) helix 4] of domain I of *A. aeolicus* RRF. The π values defined by Fauchere and Pliska (*68*) are used as hydrophobicity. C(i) are calculated from a sum of $\pi(j)\pi(j + i)$, where j runs through the sequence. The values for the (Leu-Asn-Asn-Leu-Asn-Asn-Asn)$_n$ as a model of heptad repeats are also shown (open squares). (b) Schematic diagram of three-helix bundle of domain I. Residues consisting of hydrophobic core are placed in the center of each helix. Hydrophobic residues are filled in yellow. Residues with positive charges and negative charges are filled in blue and magenta, respectively. Red circles indicate the locations of substituted residues in temperature sensitive mutants of *E. coli* RRF (*20*).

crucial role in recognition of the target molecule. Further investigation to identify the binding partner of RRF is in progress.

The structural information of the RRF molecules in solution should provide a clue to understanding the ribosome recycling and further knowledge about the translation process on the ribosome of a prokaryote. Ultimately our goal is to design an antibiotic as a specific inhibitor for the RRF molecule using this information.

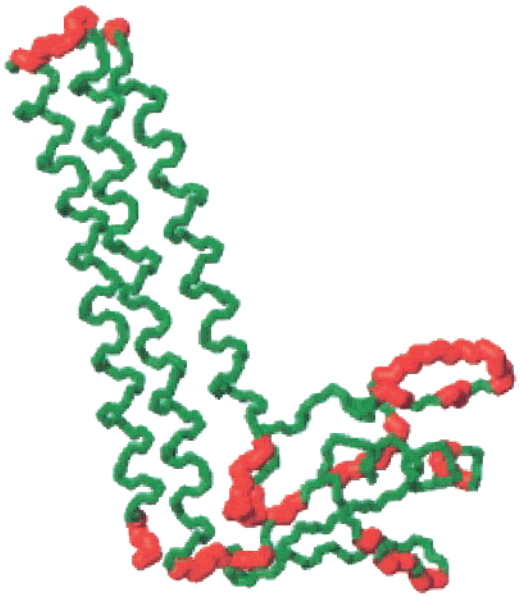

FIGURE 8: Rapid internal motion on the subnanosecond time scale for the backbone of *A. aeolicus* RRF. The trace is colored in red where the value of ^{15}N-{^{1}H} is smaller than 0.65.

ACKNOWLEDGMENT

We thank R. Huber, Universität Regensburg, for providing *A. aeolicus* genome DNA.

SUPPORTING INFORMATION AVAILABLE

One table containing backbone resonance assignments for *A. aeolicus* RRF. This material is available free of charge via the Internet at http://pubs.acs.org.

REFERENCES

1. Garrett, R. A., Douthwaite, S. R., Liljas, A., Matheson, A. T., Moore, P. B., and Noller, H. F., Eds. (2000) *The Ribosome: structure, function, antibiotics, and cellular interactions*, ASM press, Washington, DC.
2. Ban, N., Nissen, P., Hansen, J., Capel, M., Moore, P. B., and Steitz, T. A.(1999) *Nature 400*, 841−847.
3. Clemons, W. M., Jr., May, J. L. C., Wimberly, B. T., McCutcheon, J. P., Capel, M. S., and Ramakrishnan, V. (1999) *Nature 400*, 833−840.
4. Cate, J. H., Yusupov, M. M., Yuspova, G. Z., Earnest, T. N., and Noller, H. (1999) *Science 285*, 2095−2104.
5. Ban, N., Nissen, P., Hansen, J., Moore, P., and Steitz, T. (2000) *Science 289*, 905−920.
6. Wimberly, B. T., Brodersen, D. E., Clemons, W. M., Jr., Morgan-Warren, R. J., Carter, A. P, Vonrhein, G., Hartsch, T., and Ramakrishnan, V. (2000) *Nature 407*, 327−339.
7. Schluenzen, F., Tocilj, A., Zarivach, R., Harms, J., Gluehmann, M., Janell, D., Bashan, A., Bartels, H., Agmon, I., Franceschi, F., and Yonath, A. (2000) *Cell 102*, 615−623.
8. Sette, M., van Tilborg, P., Spurio, R., Kaptein, R., Paci, M., Gualerzi, C., O., Boelens, R. (1997) *EMBO J. 16*, 1436−1443.
9. Czworkowski, J., Wang, J., Steitz, T. A., and Moore, P. B. (1994) *EMBO J. 13*, 3661−3668.
10. Wang, Y., Jiang, Y., Meyering-Voss, M., Sprinzl, M., Sigler, P. B. (1997) *Nat. Struct. Biol. 4*, 650−656
11. Song, H., Mugnier, P., Das, A. K, Webb, H. M., Evans, D. R., Tuite, M. F., Hemmings, B. A., and Barford, D. (2000) *Cell 100*, 311−321.
12. Nissen, P., Kjeldgaard, M., Thirup, S., Polekhina, G., Reshetnikova, L., Clark, B. F., and Nyborg, J. (1995) *Science 270*, 1464−1472.
13. Aevarsson, A., Brazhnikov, E., Garber, M., Zheltonosova, J., Chirgadze, Y., Al-Karadadhi, S., Svensson, L. A., and Liljas, A. (1994) *EMBO J. 13*, 3669−3677.
14. Subramanian, A. R., and Davis, B. D. (1973) *J. Mol. Biol. 74*, 45−56.
15. Kaempfer, R. (1970) *Nature 228*, 534−537.
16. Kaji, A., and Hirokawa, G. (2000) Ribosome-Recycling Factor: an Essential Factor for Protein Synthesis. In *The Ribosome: Structure, Function, Antibiotics and Cellular Interactions* (Garret, R. A., Douthwaite, S. R., Liljas, A., Matheson, A. T., Moore, P. B., and Noller, H. F., Eds.) pp 527−539, ASM Press, Washington, DC.
17. Hirashima, A., and Kaji, A. (1970) *Biochem. Biophys. Res. Commun. 41*, 877−883.
18. Janosi, L., Shimizu, I., and Kaji, A. (1994) *Proc. Natl. Acad. Sci. U.S.A. 91*, 4249−4253.
19. Ryoji, M., Berland, R., and Kaji, A. (1981) *Proc. Natl. Acad. Sci. U.S.A. 78*, 5973−5977.
20. Janosi, L., Mottagui-Tabar, S., Isaksson, L. A., Sekine, Y., Ohtsubo, E., Zhang, S., Goon, S., Nelken, S., Shuda, M., and Kaji, A. (1998) *EMBO J. 17*, 1141−1151.
21. Pavlov, M. Y., Freistroffer, D. V., Heurgue-Hamard, V., Buckingham, R. H., and Ehrenberg, M. (1997) *J. Mol. Biol. 273*, 389−401.
22. Pavlov, M. Y., Freistroffer, D. V., MacDougall, J., Buckingham, R. H., and Ehrenberg, M. (1997) *EMBO J. 16*, 4134−4141.
23. Karimi, R., Pavlov, M. Y., Buckingham, R. H., and Ehrenberg, M. (1999) *Mol. Cell 3*, 601−609.
24. Hirashima, A., and Kaji, A. (1972) *J. Mol. Biol., 65*, 43−58.
25. Ogawa, K., and Kaji, A. (1975) *Eur. J. Biochem., 58*, 411−419.
26. Grentzmann, G., Kelly, P. J., Laalami, S., Shuda, M., Firpo, M. A., Cenatiempo, Y., and Kaji, A. (1998) *RNA 4*, 973−983.
27. Inokuchi, Y., Hirashima, A., Sekine, Y., Janosi, L. and Kaji, A. (2000) *EMBO J., 19*, 3788−3798.
28. Kashimori, H., Yoshida, T., Kijima, H., Shimahara, H., Uchiyama, S., Ishino, T., Shuda, M., Nakano, H., Shibata, Y., Saihara, Y., Ohkubo, T., Yoshida, T., Kaji, A., and Kobayashi, Y. (1999) *J. Biomol. NMR 15*, 341−342.
29. Selmer, M., Al-Karadaghi, S., Hirokawa, G., Kaji, A., and Liljas, A. (1999) *Science 286*, 2349−2352.
30. Kim, K. K., Min, K., and Suh S. W. (2000) *EMBO J. 19*, 2362−2370.
31. Deckert, G., Warren, P. V., Gaasterland, T., Young, W. G., Lenox, A. L., Graham, D. E., Overbeek, R., Snead, M. A., Keller, M., Aujay, M., Huber, R., Feldman, R. A., Short, J. M., Olsen, G. J., and Swanson, R. V. (1998) *Nature 392*, 353−358.
32. Piotto, M., Saudek, V., and Sklenar, V. J. (1992) *J. Biomol. NMR 2*, 661−665.
33. Kay, L. E., Keifer, P., and Saarinen, T. (1992) *J. Am. Chem. Soc. 114*, 10663−10665.
34. Wishart, D. S., Bigam, C. G., Yao, J., Abildgaard, F., Dyson, H. J., Oldfield, E., Markley, J. L., and Sykes, B. D. (1995) *J. Biomol. NMR 6*, 135−140.
35. Bax, A., Vuister, G. W., Grzesiek, S., Delaglio, F., Wang, A. C., Tschudin, R., and Zhu, G. (1994) *Methods Enzymol. 239*, 79−106.
36. Kay, L. E. (1995) *Prog. Biophys. Mol. Biol. 63*, 277−299.
37. Delaglio, F., Grzesiek, S., Vuister, G. W., Zhu, G., Pfeifer, J., and Bax, A. (1995) *J. Biomol. NMR 6*, 277−293.
38. Garrett, D. S., Powers, R., Gronenborn, A. M., and Clore, G. M. (1991) *J. Magn. Reson. 95*, 214−220.
39. Grzesiek, S., and Bax, A. (1993) *J. Am. Chem. Soc. 115*, 12593−12594.
40. Press, W. H., Teukolsky, S. A., Vettring, W. T., and Flannery, B. P. (1992) *Numerical Recipes*, Cambridge University Press, Cambridge, U.K.
41. Davis, D. G., Perlman, M. E., and London, R. E. (1994) *J. Magn. Reson. B 104*, 266−275.

42. Clore, G. M., Nilges, M., Sukumaran, D. K., Brünger, A. T., Karplus, M., and Gronenborn, A. M. (1986) *EMBO J. 5*, 2729−2735.
43. Nilges, M. (1993) *Proteins: Struct., Funct., Genet. 17*, 295−309.
44. Wüthrich, K. (1986) *NMR of Proteins and Nucleic Acids*, Wiley, New York.
45. Clore, G. M., and Gronenborn, A. M. (1991) *Science 252*, 1390−1399.
46. Cornilescu, G., Delaglio, F., and Bax, A. (1999) *J. Biomol. NMR 13*, 289−302.
47. Hu, J. S., Grzesiek, S., and Bax, A. (1997) *J. Am. Chem. Soc. 119*, 1803−1804.
48. Hu, J. S., and Bax, A. (1997) *J. Biomol. NMR 9*, 323−328.
49. Clore, G. M., Gronenborn, A. M., Szabo, A., and Tjandra, N. (1998) *J. Am. Chem. Soc. 120*, 4889−4890.
50. Brünger, A. T., Adams, P. D., Clore, G. M., DeLano, W. L., Gros, P., Grosse-Kunstleve, R. W., Jiang, J.-S., Kuszewski, J., Nilges, N., Pannu, N. S., Read, R. J., Rice, L. M., Simonson, T., and Warren, G. L. (1998) *Acta Crystallogr., Sect. D 54*, 905−921.
51. Stein, E. G., Rice, L. M., and Brünger, A. T. (1997) *J. Magn. Reson. 124*, 154−164.
52. Koradi, R., Billeter, M., and Wüthrich, K. (1996) *J. Mol. Graphics 14*, 52−55.
53. Laskowski, R. A., MacArthur, M. W., Moss, D. S., and Thornton, J. M. (1993) *J. Appl. Crystallogr. 26*, 283−291.
54. Neri, D., Szyperski, T., Otting, G., Senn, H., Wüthrich, K. (1989) *Biochemistry 28*, 7510−7516.
55. Tjandra, N., Feller, S. E., Pastor, R. W., and Bax, A. (1995) *J. Am. Chem. Soc. 117*, 12562−12566.
56. Argos, P. (1988) *Protein Eng. 2*, 101−113.
57. Tjandra, N., Garrett, D. S., Gronenborn, A. M., Bax, A., and Clore, G. M. (1997) *Nat. Struct. Biol. 4*, 443−449.
58. Tjandra, N., and Bax, A. (1997) *Science 278*, 1111−1114.
59. Atarashi, K., and Kaji, A. (2000) *J. Bacteriol. 182*, 6154−6160.
60. Ohnishi, M., Janosi, L., Shuda, M., Matsumoto, H., Hayashi, T., Terawaki, Y., and Kaji, A. (1999) *J. Bacteriol. 181*, 1281−1291.
61. Fujiwara, T., Ito, K., Nakayashiki, T., and Nakamura, Y. (1999) *FEBS Lett. 447*, 297−302.
62. Lupas, A. (1996) *Trends Biochem. Sci. 21*, 375−382.
63. Xiao, L., and Honig, B. (1999) *J. Mol. Biol. 289*, 1435−1444.
64. Jaenicke, R., and Bohm, G. (1998) *Curr. Opin. Struct. Biol. 8*, 738−748.
65. Janosi, L., Mori, H., Sekine, Y., Abragan, J., Janosi, R., Hirokawa, G., and Kaji, A. (2000) *J. Mol. Biol. 295*, 815−829.
66. Feher, V. A., and Cavanagh, J. (1999) *Nature 400*, 289−293.
67. Ishima, R., Freedberg, D. I., Wang, Y. X., Louis, J. M., and Torchia, D. A. (1999) *Struct. Fold Des. 7*, 1047−1055.
68. Fauchere, J. L., and Pliska, V. (1983) *Eur. J. Med. Chem. 18*, 369−375.

BI002474G